Structure Development and Melt Viscoelastic Properties of PE/Organoclay Nanocomposite Blown Films

Mehdi H. Abdolrasouli, Ehsan Behzadfar, Hossein Nazockdast, Farhad Sharif

Department of Polymer Engineering, Amirkabir University of Technology, Tehran, Iran

Received 19 April 2011; accepted 15 November 2011
DOI 10.1002/app.36510
Published online 22 January 2012 in Wiley Online Library (wileyonlinelibrary.com).

ABSTRACT: The effects of compatibilizer and the type of polyethylene (PE) matrix on structure development of PE/organoclay nanocomposite samples were investigated by means of X-ray diffraction technique and transmission electron microscopy in conjunction with melt viscoelastic measurements. It was shown that the presence of compatibilizer plays a key role in determining the extent of intercalation and resulting structure development in both linear low-density polyethylene (LLDPE) and low-density polyethylene (LDPE). The LLDPE/organoclay nanocomposite samples exhibited a pronounced low-frequency nonterminal storage modulus whose values were found to be greater than those of LDPE/organoclay nanocomposite samples. The percentage increase in storage modulus values for the compatibilized LLDPE/organoclay nanocomposite sample compared to the virgin LLDPE sample was 1080, while the percentage increase in storage modulus values for the compatibilized LDPE/organoclay nanocomposite sample compared to the virgin LDPE sample was 200, at frequency 0.1 s^{-1}. The melt viscoelastic measurements performed on the nanocomposite blown film samples indicated that at higher draw-down ratio the organoclay platelets and/or tactoids were aligned in the flow direction. Comparing the melt viscoelastic results obtained for annealed and unannealed nanocomposite blown film samples, it was demonstrated that the reorientation of the induced organoclay alignment, which led to network structure formation in the amorphous phase of PE, is very slow, and the time required to complete the reorientation was found to be longer than 3 h at annealing temperature (100°C). © 2012 Wiley Periodicals, Inc. J Appl Polym Sci 125: E435–E444, 2012

Key words: nanocomposites; polyethylene; organoclay; rheology; films

INTRODUCTION

Polyolefins, due to their excellent processability, high chemical resistance and desirable physical properties have received the most attention from packaging industry to greenhouse covering application. During the last two decades, extensive research activities have been directed toward polyolefin/organoclay nanocomposites, with very low organoclay loading, because of their enhanced barrier and greenhouse effect, flame retardancy, and mechanical properties compared to the conventional composites.[1–5] To achieve polyolefin/organoclay with optimum properties, a well-developed structure is usually required. On the other hand, it is usually a difficult task to produce polyolefin/organoclay nanocomposites with desirable structure, due to the very week interactions of hydrophobic polyolefins with the polar surface of the organoclays.[6–8] Thus, modified polymers having polar groups, called as compatibilizers or interfacial agents must be introduced in nanocomposite formulations to enhance the extent of intercalation as well as dispersion of organoclay in polyolefin matrix. In most research works carried out on polypropylene/organoclay nanocomposites prepared by the melt compounding, the maleic anhydride-grafted polypropylene was used as compatibilizer which led to form an intercalated and/or exfoliated structure.[9–12] However, few studies focused on polyethylene/organoclay nanocomposite samples have shown less degree of success in increasing interlayer *d*-spacing and structure development compared to the polypropylene-based nanocomposites.[13,14]

In polymer/organoclay nanocomposites, the extent of intercalation and degree of dispersion of organoclay can be evaluated by X-ray diffraction (XRD) along with transmission electron microscopy (TEM). Although XRD offers a convenient method to determine the interlayer spacing in the original organoclay layers and intercalated structure, little information can be obtained about the spatial distribution of organoclay layers and/or any disordered structure. In contrast to XRD, TEM provides very useful information about the dispersion state of organoclay particles in a wide range of length scales, but it is a time-consuming and expensive technique.

The measurement of rheological behavior of polymeric materials in the molten state is crucial to gain

Correspondence to: H. Nazockdast (nazdast@aut.ac.ir).

© 2012 Wiley Periodicals, Inc.

TABLE I
Some Properties of Material Used in This Study

Material	Specification	Trade name and Supplier
Low-density polyethylene, LDPE	MFI[a] = 2 g/10 min Specific gravity = 0.922 g cm^{-3} Melting point = 113°C	HP2022, Saudi Basic Industries Corporation (SABIC), Kingdom of Saudi Arabia.
Linear low-density polyethylene, LLDPE	MFI[a] = 2 g/10 min Specific gravity = 0.918 g cm^{-3} Melting point = 123°C	218W, Saudi Basic Industries Corporation (SABIC), Kingdom of Saudi Arabia.
Maleic anhydride grafted linear low-density polyethylene, LL-*g*-MA	MFI[a] = 1.2 g/10 min Specific gravity = 0.918 g cm^{-3} Melting point = 123°C	Orevac® 18302n, Arkema, France.
Nanofiler	d_{001} spacing = 3.15 nm, Specific gravity = 1.66, dihydrogenated tallow[b] (2M2HT) quaternary ammonium salt[c] Organic content = 43%	Cloisite® 15A, Southern Clay Products, Inc.[24]

[a] By ASTM D 1238 (190°C, 2.16 kg).
[b] Tallow is a natural product composed predominantly (63%) of saturated and unsaturated C18 chains. HT is the saturated form yet contains a small fraction of double bonds.
[c] The modifier concentration describes the number of milliequivalents of amine salt used per 100 g of clay (MER) during the cation exchange reaction with sodium montmorillonite.

fundamental understanding of their processability undergoing processes like film processing. In the case of polymer-layered silicate nanocomposites, melt-rheological properties offer great insight into understanding existing structure as well as structural changes occurring during the processing. Thus, the rheology can be used as a powerful method in complementary to XRD and TEM to study structure of polymer/organoclay nanocomposites.[15–19]

Film is the largest market segment for polyethylene (PE). PE films are used for food, good, and farming packaging, garbage bags, greenhouses covering, liners, and merchandise packaging. Improvements in properties of the PE films with incorporation of organoclay can promote current applications and even more advanced applications like electronic and pharmaceutical packaging.[3] On the other, the ability of a polyethylene to be converted into film depends on its melt strength or equivalent rheological properties, like the elongational viscosity and viscoelastic behavior that can be affected by incorporation of organoclay.[20]

The literature shows few work focusing on the influence of draw-down ratio (DDR) and annealing treatment on structure development of the nanocomposite films and flow-induced orientation of organoclay in nanocomposite. Kaito et al.[21] showed that the orientation function of liquid crystal polymer markedly increases with increasing draw-down ratio, but the increase saturates at higher DDR. They also showed that the molecular orientation was relaxed by annealing at high temperature. Lotti et al.[20] indicated that high-density polyethylene/organoclay nanocomposite blown film processed in higher elongation had an instable morphology and displayed a high-stress overshooting. Shah et al.[22] demonstrated that the increase of DDR reduced the gas permeability of an ionomer/organoclay nanocomposite film due to a higher biaxial orientation of the organoclay platelets in the plane of the film, but the variation of blown-up ratio did not interfere. Golebiewski et al.[23] demonstrated that blown films of LDPE/organoclay with higher blown-up ratio are characterized by slightly worse mechanical properties but have improved barrier properties as compared to films from pristine polyethylene and to blown films at lower blown-up ratio. However, the effects of DDR and annealing process on structure of the nanocomposite film have not clearly been understood.

The aim of this work was to provide more insight into understanding the effect of polyethylene matrix molecular structure and compatibilizer on structure development in PE/organoclay nanocomposite and the effect of DDR and annealing process on structure development in nanocomposite blown film samples, by means of XRD technique and linear and nonlinear melt viscoelastic measurements.

EXPERIMENTAL PART

Materials

Table I provides some information about the material used in this study. Linear low-density polyethylene (LLDPE) and low-density polyethylene (LDPE) were used as the polymer matrices of the nanocomposites. A commercial maleic anhydride grafted Linear low-density of polyethylene, LL-*g*-MA, used as compatibilizer. Cloisite 15A which is a natural montmorillonite modified with a quaternary

TABLE II
The Compositions Details of the Samples

Samples	LLDPE (wt %)	LDPE (wt %)	Cloisite 15A (wt %)	LL-*g*-MA (wt %)
LL4	96	–	4	0
LLC4	88	–	4	8
LD4	–	96	4	0
LDC4	–	88	4	8

ammonium salt was chosen as nanofiller to prepare nanocomposite.

Melt compounding

LLDPE/organoclay and LDPE/organoclay nanocomposite samples with composition as listed in Table II were considered. All the samples were prepared in a corotating twin-screw extruder (Brabender). The temperature of the extruder was maintained at 150, 160, 170, 180, 180, and 180°C from hopper to the die and the screw speed was fixed at 150 rpm. Compatibilized LLDPE/organoclay nanocomposite sample was converted into films by using a single-screw extruder (Plasti-corder PL200) equipped with blown die and film take-up device in two different of DDR, 10 and 20. The temperatures of the three heating zones and the die of the single-screw extruder were 180, 190, 190, and 190°C, and the screw speed was 30 rpm. Blown film nanocomposite samples were annealed at 100°C for 3 h.

Characterization

X-Ray diffraction curves of the samples were recorded on a Rigaku X-ray diffractometer with nickel filtered Cu-Kα radiation (λ = 0.154 nm) operated at 50 Kv and 150 Ma. Data were obtained over the range 2θ = 1.5°–10°.

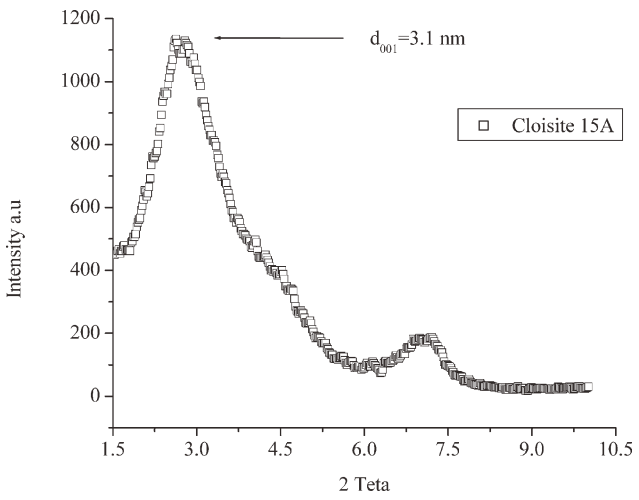

Figure 1 X-Ray diffraction result of the Cloisite 15A.

TEM images were obtained at 160 kV, with a JEOL/JEM-2000 FX electron microscope.

The rheological measurement of the samples were studied by using a rheometric mechanical spectrometer (Paar Physica USD200), with a parallel plate (diameter = 2.5 cm; gap = 1 mm) geometry at 175°C and at strain of 1% to ensure the linear viscoelastic region. Linear melt-state viscoelastic behavior of the samples was studied using frequency sweep experiment in small strain oscillatory shear deformations. The nonlinear rheological behavior of these materials was investigated by employing start-up of steady shear flow. In the start-up of steady-shear flow experiments, the samples were imposed to a constant shear rate (hear $\dot{\gamma} = 0.1\,s^{-1}$), and the transient stress was monitored with time.

RESULTS AND DISCUSSION

Characterization of the mixtures

XRD results

Figure 1 shows the X-ray diffraction pattern of the Cloisite 15A. As it can be seen, the organoclay shows two characteristic diffraction peaks at 2θ = 2.81° and 2θ = 7.3°, corresponding to *d*-spacing of 3.15 and 2 nm, respectively. The peak observed at 2θ = 2.81° corresponds to the interlayer spacing of the surface modified layers of montmorillonite and that observed at 2θ = 7.3° is related to the unmodified layers.

Figure 2 compares the X-ray diffraction results of the organoclay, compatibilized and uncompatibilized LLDPE/organoclay nanocomposite samples containing 4 wt % organoclay. It can be noticed that the sample containing compatibilizer (LLC4) exhibits only one broad peak with very low intensity at 2θ = 2.6°,

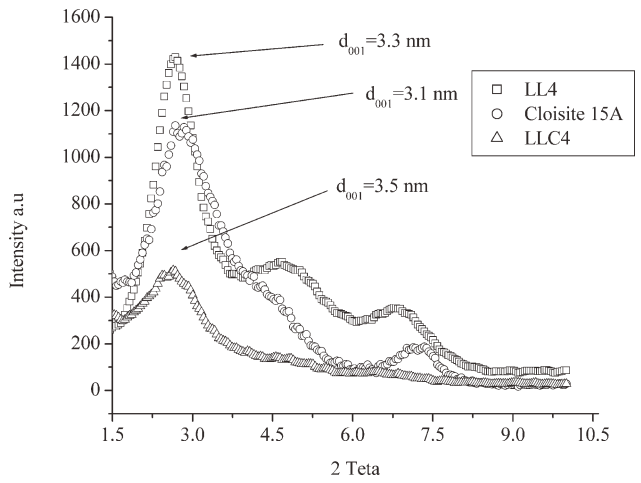

Figure 2 X-Ray diffraction results of organoclay (○), compatibilized (Δ), and uncompatibilized (□) LLDPE-based nanocomposite samples.

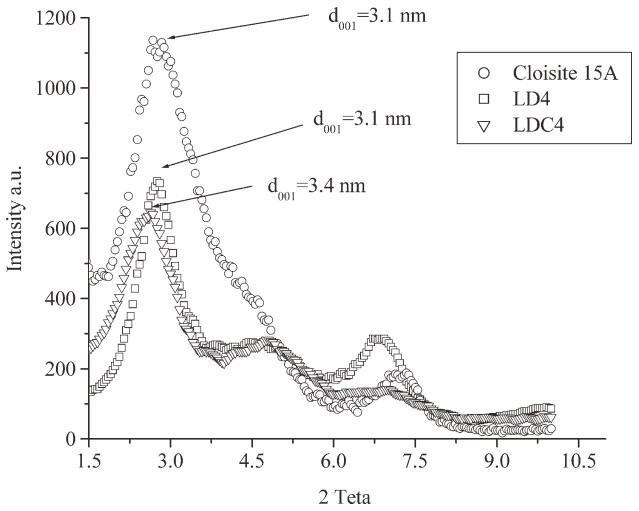

Figure 3 X-Ray diffraction results of organoclay (○), compatibilized (□), and uncompatibilized (□) LDPE-based nanocomposite samples.

corresponding to *d*-spacing of 3.5 nm. The shifting to lower angles and broadening of this characteristic diffraction peak suggests an increase in interlayer spacing of the organoclay, which is referred to as intercalation. Figure 2 also shows that the uncompatibilized LLDPE sample (LL4), exhibits three peaks: first peak at $2\theta = 2.8°$, identical to that observed for organoclay, an additional peak approximately at $2\theta = 4.8°$, missing in Cloisite15A diffractogram and third peak at $2\theta = 7°$, slightly shifted in comparison with that of organoclay (7.3°). The first diffraction peak of this sample is more intense and sharper as compared to the reflection of the pristine organoclay. This indicates a well-ordered structure in which the interlayer distance is almost constant for all the tactoids-containing modifying group. This, probably, can be attributed to the interlayer reorganization during the melt intercalation of the polymeric chains.[25] The additional peak observed in the uncompatibilized sample may be attributed to the organoclay with reduced interlayer spacing, resulted from degradation of organoclay modifying groups and/or their removal from surface of organoclay. The slight shift in the third XRD peak of uncompatibilized sample indicates increasing in *d*-spacing of unmodified layer which can be attributed to the penetration of the removed organoclay modifying groups from organoclay surface into the interlayer space of unmodified layer.

Comparing the XRD results of compatibilized and uncompatibilized LLDPE/organoclay reveals that the LLDPE matrix is not capable enough to penetrate into interlayer *d*-spacing of organoclay particles and using of LL-*g*-MA is almost essential for melt intercalation.

Figure 3 shows the X-ray diffraction results of the organoclay, compatibilized and uncompatibilized LDPE/organoclay nanocomposite samples containing 4 wt % organoclay. It can be seen that, diffraction peaks of the uncompatibilized sample is narrower than that of compatibilized sample, suggesting that the structure of the sample without compatibilizer is a more ordered structure than that of the sample with compatibilizer. These results also show that main diffraction peak of compatibilized sample shifts to lower angle suggesting increased *d*-spacing due to

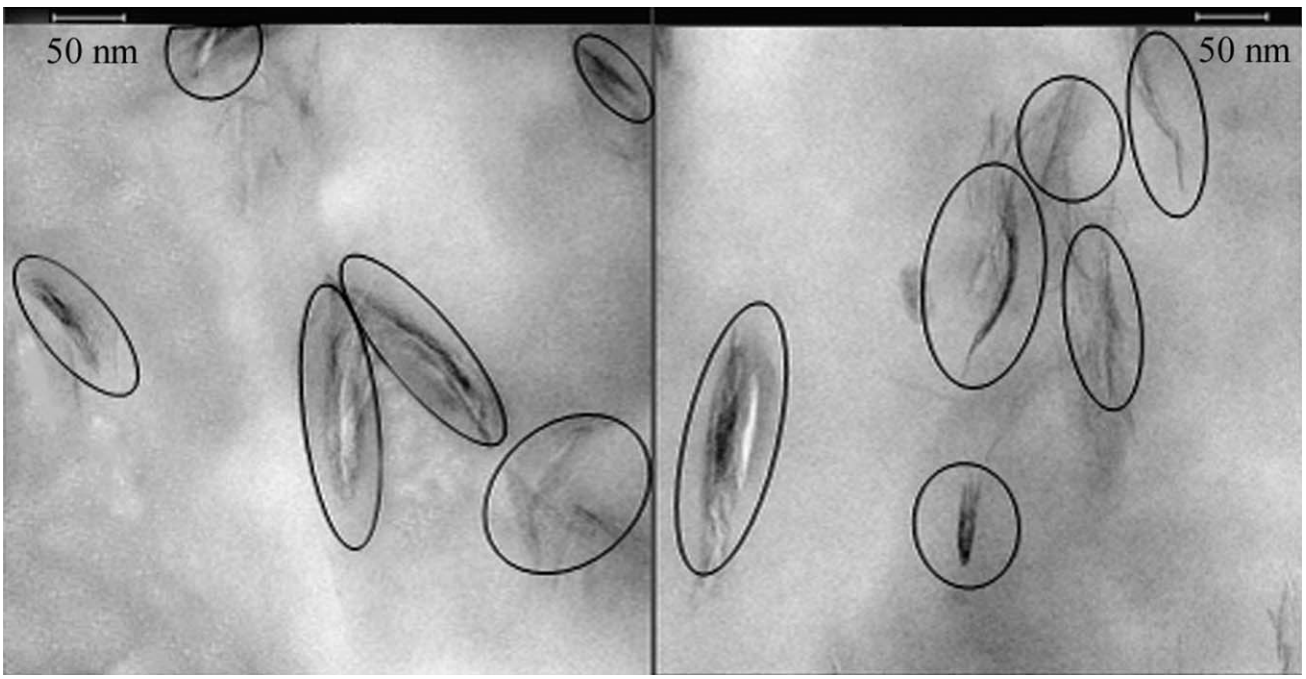

Figure 4 TEM micrographs of compatibilized LLDPE/organoclay nanocomposite sample.

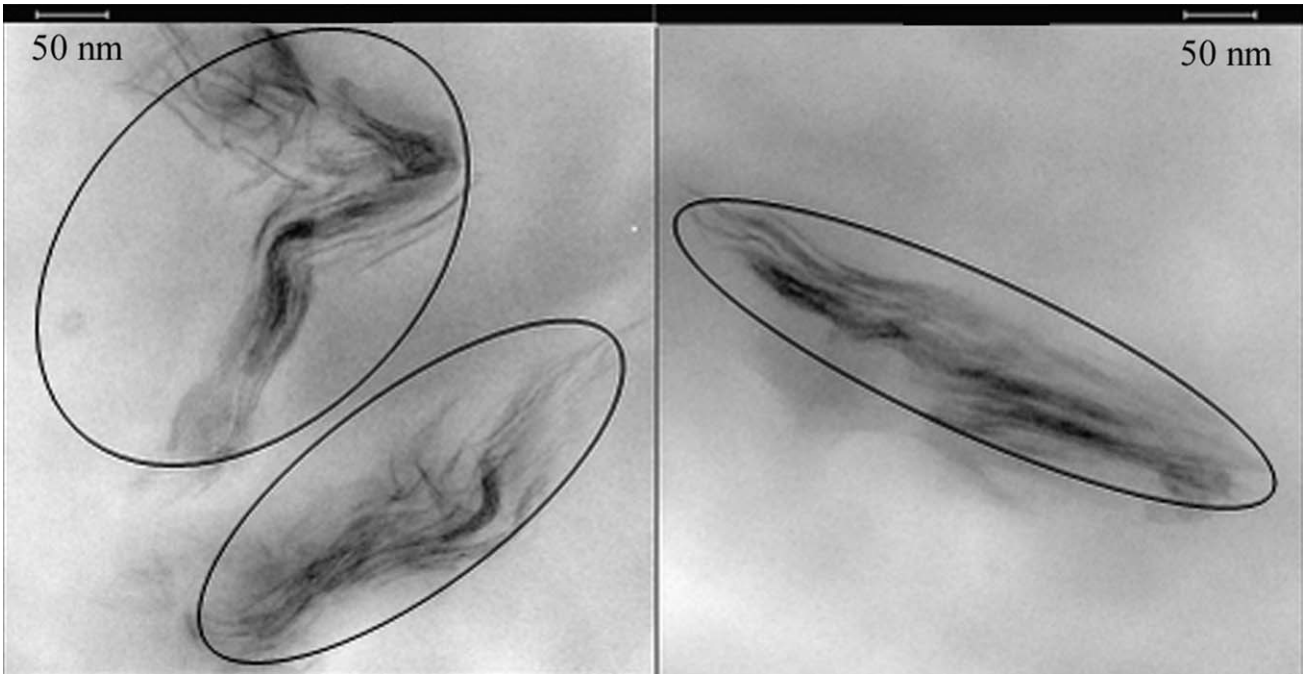

Figure 5 TEM micrographs of compatibilized LDPE/organoclay nanocomposite sample.

the stronger interaction between LDPE containing LL-*g*-MA sample and organoclay.

By comparing the results shown in Figures 2 and 3 one may notice that, in compatibilized LDPE/organoclay nanocomposite sample the extent of melt intercalation is lower than that in compatibilized LLDPE/organoclay nanocomposite sample. This could be attributed to hindrance effect of long chain branches of LDPE matrix and lower compatibility between LDPE and LL-*g*-MA compatibilizer.

TEM results

Figures 4 and 5 show typical TEM micrographs of the LLDPE/organoclay and LDPE/organoclay nanocomposite samples both compatibilized with LL-*g*-MA. As can be observed the average number of clay particles in compatibilized LLDPE/organoclay and LDPE/organoclay nanocomposite samples is 12/2 and 3/2, respectively. Considering the fact that surface area of these TEM micrographs is about 0.20 μm^2, the average number of organoclay particles per surface area unit (μm^2) would be about 30 and 7.5, respectively. The greater average number of organoclay particles per surface area unit (μm^2) of LLDPE/organoclay suggests better dispersion which is in agreement whit the XRD results discussed earlier. A quantification of the exfoliation degree would be relevant, through the concept of specific particle density, which is the number of organoclay entities (particles) per surface area unit (μm^2) divided by the organoclay weight fraction. These results showed that the specific particle density which is related to the degree of exfoliation and/or intercalation, in compatibilized LLDPE/organoclay and compatibilized LDPE/organoclay are about $30/0.04 = 750$ and $7.5/0.04 = 187.5$, respectively.

Rheological results

Figure 6 shows the storage modulus (G') as a function of frequency for virgin LLDPE (LLg), the melt processed LLDPE (LL), uncompatibilized (LL4), and compatibilized LLDPE/organoclay nanocomposite sample (LLC4). Table III shows storage modulus values and percentage increase in storage modulus

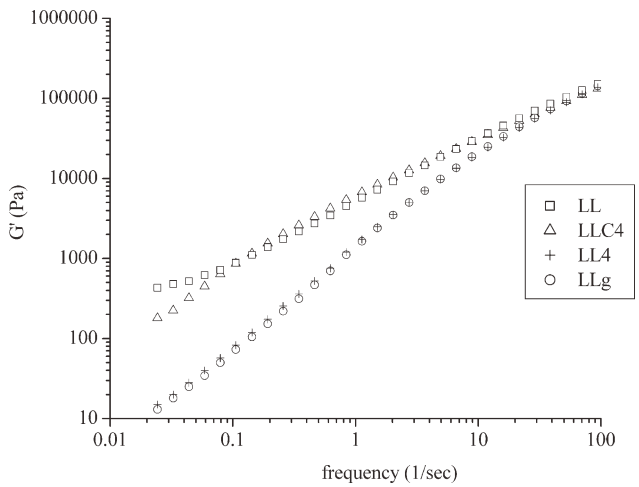

Figure 6 Storage modulus (G') versus frequency (ω) of LLDPE and LLDPE/organoclay nanocomposite samples at 175°C.

TABLE III
Storage Modulus Values and Percentage Increase in Storage Modulus Values for Some Samples, at Frequency 0.1 s^{-1}

Samples	G'[a]	Percentage change in G'
LLg	73	
LL	885	$\frac{\bar{G}'_{LL}-G'_{LLg}}{G'_{LLg}} \times 100 \approx 1110$
LL4	82.8	$\frac{G'_{LL4}-G'_{LLg}}{G'_{LLg}} \times 100 \approx 0$
LLC4	863	$\frac{G'_{LLC4}-G'_{LLg}}{G'_{LLg}} \times 100 \approx 1082$

[a] Storage modulus at frequency 0.1 s^{-1} [pa].

values for these samples compared to the LLg, at frequency 0.1 s^{-1}.

These results show that melt processing of LLDPE granule at absence of organoclay increases the storage modulus values particularly at low-frequency range (ca. 1110% at frequency 0.1 s^{-1}) as a result of chain branching and/or gel formation. It can be seen in the Figure 6 that the results of G' versus frequency obtained for uncompatibilized LLDPE/organoclay nanocomposite samples is almost superimposed with that of virgin LLDPE. This suggests that presence of organoclay can act as an inhibitor and prevents the degraded chain leading to branching and/or gel formation. These results also show that while the uncompatibilized LLDPE/organoclay nanocomposite samples exhibits similar viscoelastic behavior as that of LLDPE matrix, the compatibilized LLDPE/organoclay nanocomposite samples show a pronounced low-frequency nonterminal behavior of storage modulus (presence of organoclay in compatibilized LLDPE/organoclay nanocomposite sample increases the storage modulus values about 1080% at frequency 0.1 s^{-1}). This can be considered as indication of three-dimensional (3D) network structure formed in the compatibilized LLDPE/organoclay nanocomposite samples as a result of greater extent of intercalation and better dispersion of organoclay in uncompatibilized LLDPE/organoclay nanocomposite samples compared to the uncompatibilized LLDPE/organoclay nanocomposite samples.

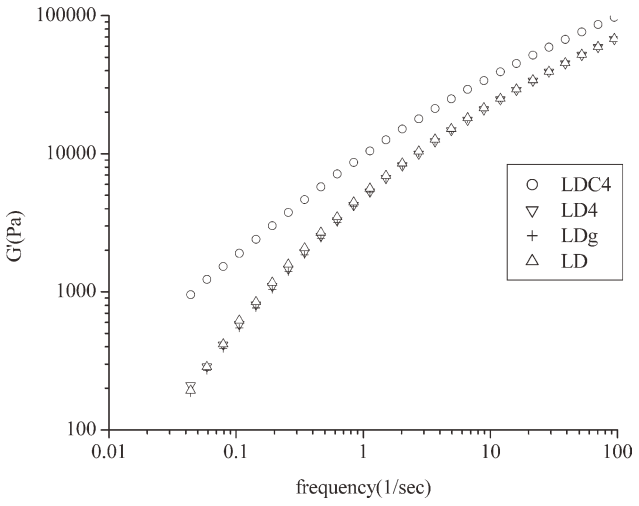

Figure 7 Storage modulus (G') versus frequency (ω) of LDPE and LDPE/organoclay nanocomposite samples at 175°C.

The results of similar experiment obtained for virgin LDPE (LDg), the melt processed LDPE (LD), uncompatibilized (LD4), and compatibilized LDPE/organoclay nanocomposite samples (LDC4) are shown in Figure 7. Table IV shows storage modulus values (G') and percentage increase in storage modulus values for these samples compared to the virgin LDPE (LDg), at frequency 0.1 s^{-1}. These results show while the uncompatibilized LDPE/organoclay nanocomposite sample (LD4), and the melt-processed LDPE (LD) exhibits similar viscoelastic behavior as that of virgin LDPE (LDg), the compatibilized LDPE/organoclay nanocomposite sample (LDC4) shows 200% increase in storage modulus values at frequency 0.1 s^{-1}. By comparing these results with those shown in Figure 7 and Table IV one may notice that, in LDPE in contrast to LLDPE, melt process has no significant effect on increasing the low-frequency storage modulus, suggesting a negligible chain branching in LDPE. These results also show that the extent of 3D network structure formation in LDPE/organoclay nanocomposite sample is lower than that in LLDPE/organoclay nanocomposite sample. This could be attributed to hindrance effect of long chain branches of LDPE matrix and lower compatibility between LDPE and LL-*g*-MA compatibilizer.

Characterization of the blown film samples

XRD results

In Figure 8, there are reported the X-ray diffraction results of compatibilized LLDPE/organoclay nanocomposite blown films samples and sample before converting into film (LLC4). It can be seen that characteristic peak of nanocomposite film samples intensifies and slightly shifts to lower angle (from

TABLE IV
Storage Modulus Values and Percentage Increase in Storage Modulus Values for Some Samples, at Frequency 0.1 s^{-1}

Samples	G'[a]	Percentage change in G'
LDg	611	
LD	621	$\frac{\bar{G}'_{LD}-G'_{LDg}}{G'_{LDg}} \times 100 \approx 0$
LD4	615	$\frac{G'_{LD4}-G'_{LDg}}{G'_{LDg}} \times 100 \approx 0$
LDC4	1900	$\frac{G'_{LDC4}-G'_{LDg}}{G'_{LDg}} \times 100 \approx 200$

[a] Storage modulus at frequency 0.1 s^{-1} [pa].

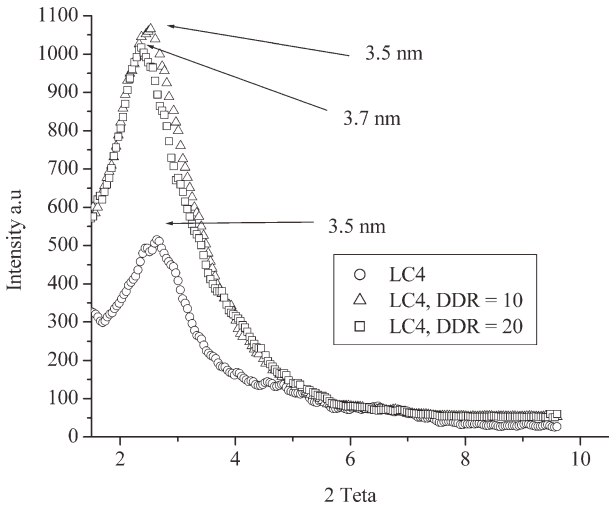

Figure 8 X-Ray diffraction of nanocomposite blown film samples.

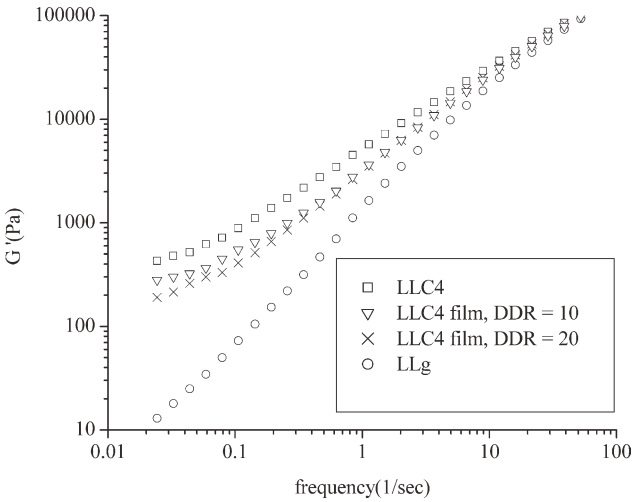

Figure 9 Storage modulus (G') versus frequency (ω) of the nanocomposite blown film samples at 175°C.

$2\theta = 2.6°$ to $2\theta = 2.37°$) as DDR increases (from 10 to 20, respectively). From these results, it can be concluded that film-blowing process leads to organoclay orientation in the film samples while the interlayer distance of organoclay also increases.

Rheological results

Figure 9 shows the results of storage modulus measured as a function of frequency for the compatibilized LLDPE/organoclay nanocomposite blown film samples. Similar results obtained for LLDPE matrix (LLg) and compatibilized LLDPE/organoclay nanocomposite blown film samples before converting into the film (LLC4) are also shown in Figure 9. Table V shows storage modulus values (G') and percentage change in storage modulus values for these samples compared to the LLC4, at frequency 0.1 s^{-1}. It is clearly seen that, with increasing the DDR from 10 to 20, the low-frequency storage modulus values of blown film LLC4 sample at frequency 0.1 s^{-1} decreased from −37% to −53% as a result of weakening of network structure formed between organoclay.

The subsequent disorientation of organoclay domains and the resulting effect on the rheological properties can provide interesting information regarding the structure evolution in nanocomposite blown film samples. Thus, the nanocomposite blown film samples were annealed at 100°C for 3 h, and the frequency sweep experiments was repeated on these samples. As it is observed in Figures 10 and 11 and Table VI, the annealing process can increase low-frequency storage modulus values of the both blown film LLC4 samples with DDR 10 and 20 (about 14 and 31% at frequency 0.1 s^{-1}, respectively), as a result of organoclay disorientation leading to stronger network formation.

Figures 12 and 13 and Table VII show the results of transient stress in start-up of steady shear flow experiment for LLDPE/organoclay nanocomposite blown film samples containing 4 wt % organoclay before and after annealing at 100°C for 3 h. These results clearly indicate that increase in draw-down ratio has a pronounced effect on decreasing the stress overshoot of the sample (Percentage decrease in stress overshoot for blown film LLC4 sample with DDR 10 and 20 compared to the sample before converted into the film is −27% and −47%, respectively). This reveals that the organoclay platelets and/or tactoids are aligned in the preferred direction dictated by the flow field in the freeze line and

TABLE V
Storage Modulus Values and Percentage Decrease in Storage Modulus Values for Some Samples, at Frequency 0.1 s^{-1}

Samples	G'[a]	Percentage change in G'
LLC4	885	
Blown film LLC4, DDR = 10	550	$\frac{G'_{\text{Blown film LLC4, DDR=10}} - G'_{\text{LLC4}}}{G'_{\text{LLC4}}} \times 100 \approx -37$
Blown film LLC4, DDR = 20	410	$\frac{G'_{\text{Blown film LLC4, DDR=20}} - G'_{\text{LLC4}}}{G'_{\text{LLC4}}} \times 100 \approx -53$

[a] Storage modulus at frequency 0.1 s^{-1} [pa].

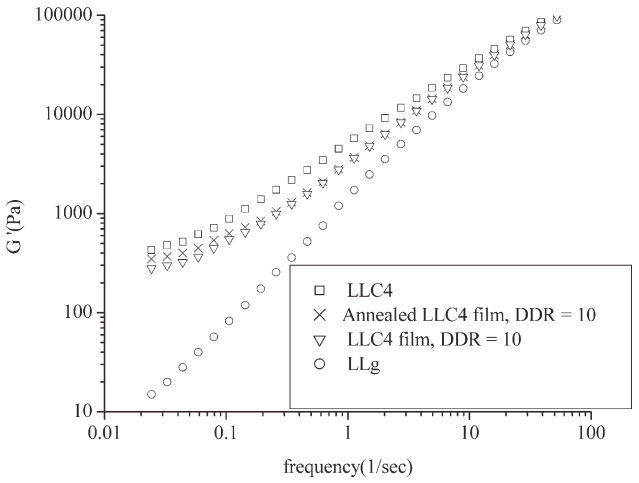

Figure 10 Storage modulus (G') versus frequency (ω) of the nanocomposite blown film samples at 175°C for samples with DDR = 10 after and before annealing.

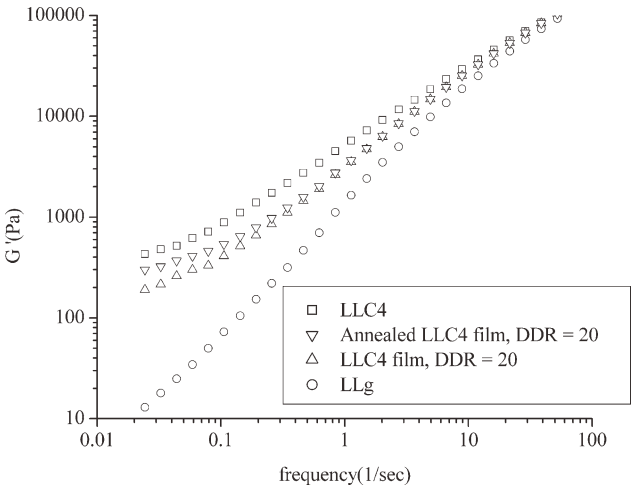

Figure 11 Storage modulus (G') versus frequency (ω) of the nanocomposite blown film samples at 175°C for samples with DDR = 20 after and before annealing.

TABLE VI
Storage Modulus Values and Percentage Increase in Storage Modulus Values for Some Samples, at Frequency 0.1 s^{-1}

Samples	G'[a]	Percentage change in G'
Blown film LLC4, DDR = 10	550	
Annealed LLC4 film, DDR = 10	630	$\frac{G'_{\text{Anneealed film LLC4, DDR=10}} - G'_{\text{Blown film LLC4, DDR=10}}}{G'_{\text{LLC4}}} \times 100 \approx 14$
Blown film LLC4, DDR = 20	410	
Annealed LLC4 film, DDR = 20	540	$\frac{G'_{\text{Anneealed film LLC4, DDR=20}} - G'_{\text{Blown film LLC4, DDR=20}}}{G'_{\text{LLC4}}} \times 100 \approx 31$

[a] Storage modulus at frequency 0.1 s^{-1} [pa].

frozen-in during the solidification of film blowing process. As it can be noticed, the annealed nanocomposite blown film samples showed an appreciable increase in low-frequency storage modulus along with a pronounced increased stress overshoot as a result of reorientation of the organoclay platelets

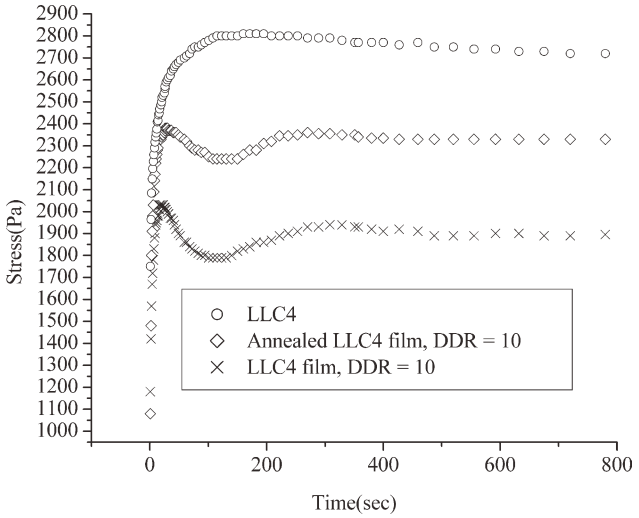

Figure 12 Transient shear stress versus time in start-up of steady shear follow experiment carried out on nanocomposite blown film sample with DDR = 10 before and after annealing.

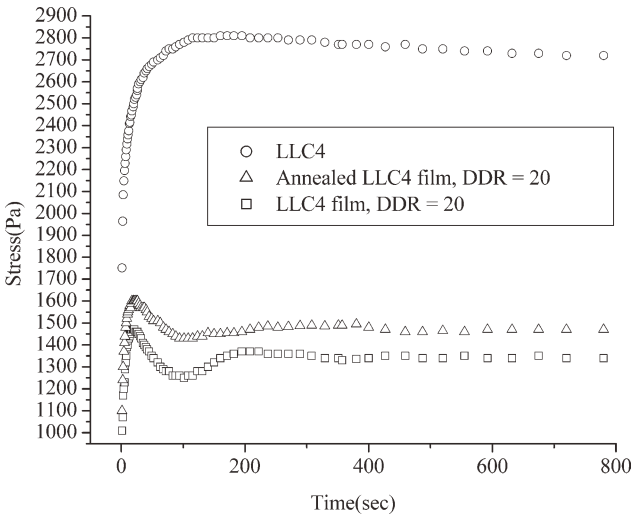

Figure 13 Transient shear stress versus time in start-up of steady shear follow experiment carried out on nanocomposite blown film sample with DDR = 20 before and after annealing.

TABLE VII
Stress Overshoot Values and Percentage Change in Stress Overshoot Values for some samples

Samples	τ_s[a]	Percentage change in stress overshoot values
LLC4	2810	
LLC4 film, DDR = 10	2030	$\frac{\bar{\tau}_{s\ \text{Blown film LLC4, DDR=10}} - \tau_{s\ \text{LLC4}}}{\tau_{s\ \text{LLC4}}} \times 100 \approx -27$
Annealed LLC4 film, DDR = 10	2360	$\frac{\tau_{s\ \text{Annealed film LLC4, DDR=10}} - \tau_{s\ \text{film LLC4, DDR=10}}}{\tau_{s\ \text{film LLC4, DDR=10}}} \times 100 \approx 16$
LLC4 film, DDR = 20	1490	$\frac{\tau_{s\ \text{Blown film LLC4, DDR=20}} - \tau_{s\ \text{LLC4}}}{\tau_{s\ \text{LLC4}}} \times 100 \approx -47$
Annealed LLC4 film, DDR = 20	1630	$\frac{\tau_{s\ \text{Annealed film LLC4, DDR=20}} - \tau_{s\ \text{film LLC4, DDR=20}}}{\tau_{s\ \text{film LLC4, DDR=20}}} \times 100 \approx 9$

[a] Stress overshoot [pa].

and/or tactoids in the favor of network structure formation (the annealing process increases stress overshoot of blown film LLC4 sample with drawdown ratio 10 and 20 about 16 and 9%, respectively). The time required for reorientation of organoclay platelet and/or tactoids was found to be very long depending on the annealing temperature ($t >> 2000$ s at 100°C), and therefore, the relaxation of polymer matrix molecules could hardly affect the reorientation of organoclay. These result show, flow induced orientation of organoclay in the nanocomposite blown film samples is not thermodynamically stable and can be changed in to disorientation state in the amorphous phase of polyethylene ($T_g = -100$°C), during the long-time services. These results are in agreement with those reported by Nazockdast et al.[26] who suggested that the rotation of organoclay platelets and/or tactoids can also play a role in determining the stress overshoot exhibited by nanocomposite materials.

CONCLUSIONS

From TEM, XRD, and melt linear viscoelastic results obtained for LLDPE and LDPE-based nanocomposite samples; it was shown that the long chain branches of LDPE matrix has an appreciable hindrance effect on reducing the efficiency of melt intercalation and resulting structure development compared to the LLDPE matrix. The results of nonlinear melt viscoelastic measurement (transient shear-stress test) performed on the nanocomposite blown film samples showed a decrease of stress overshoot with increasing a DDR as a result of flow induced alignment of the organoclay platelets and/or tactoids. This was evidenced by the result, obtained from the annealed nanocomposite blown film samples which showed disorientation and restructuring leading to formation of 3D network between organoclay platelets and/or tactoids (the annealing process increases stress overshoot of blown film LLC4 sample with DDR 10 and 20 about 16 and 9%, respectively). These results were in agreement with decreasing the low-frequency storage modulus with increasing the drawdown ratio used to produce nanocomposite blown film samples (as the DDR increases from 10 to 20, low-frequency storage modulus values of these sample at frequency 0.1 s^{-1} decreases from −37% to −53%). From these results, it was concluded that rotation of organoclay platelet and/or tactoids has an appreciable contribution in determining the stress overshoot of the nanocomposite film samples along with hydrodynamic forces and network breakdown.

References

1. Min, K. D.; Kim, M. Y.; Choi, K.; Lee, J. H.; Lee, S. Polym Bull 2006, 57, 101.
2. Scaffaro, R.; Botta, L.; La Mantia, F. P. Macromol Mater Eng 2009, 294, 445.
3. Zhong, Y.; Janes, D.; Zheng, Y.; Hetzer, M.; Kee, D. D. Polym Eng Sci 2007, 47, 1101.
4. Ton-That, M.; Perrin-Sarazin, F. Polym Eng Sci 2004, 44, 1212.
5. Sanchez, V.; Lopez, Q. Macromol Mater Eng 2006, 291, 128.
6. Morawiec, J.; Pawlak, A.; Slouf, M.; Galeski, A.; Piorkowska, E.; Krasnikowa, N. Eur Polym J 2005, 41, 1115.
7. Médéric, P.; Razafinimaro, T.; Aubry, T.; Moan, M.; Klopffer, M. Macromol Symp 2005, 221, 75.
8. Malucelli, G.; Ronchetti, S.; Lak, N.; Priola, A.; Dintcheva, N. T.; La Mantia, F. P. Eur Polym J 2007, 43, 328.
9. Wang, K.; Liang, S.; Deng, J.; Yang, H.; Zhang, Q.; Fu, Q.; Dong, X.; Wang, D.; Han, C. Polymer 2006, 47, 7131.
10. Lertwimolnun, W.; Vergnes, B. Polymer 2005, 46, 3462.
11. Wang, Y.; Chen, F. J Appl Polym Sci 2005, 97, 1667.
12. Lopez, Q.; Sanchez, V. J Appl Polym Sci 2006, 100, 4748.
13. La Mantia, F. P.; Dintcheva, N. T. J Appl Polym Sci 2006, 102, 4749.
14. Hotta, S.; Paul, D. Polymer 2004, 45, 7639.
15. Médéric, P.; Razafinimaro, T.; Aubry, T. Polym Eng Sci 2006, 46, 989.
16. Lee, K.; Han, C. Macromolecules 2003, 36, 804.
17. Krishnamoorti, R.; Giannelis, E. Macromolecules 1997, 30, 4097.
18. Urekli, K.; Karim, A.; Amis, E.; Krishnamoorti, R. Macromolecules 2004, 37, 507.

19. Ren, J.; Silva, A.; Krishnamoorti, R. Macromolecules 2000, 33, 3739.
20. Lotti, C.; Isaac, C.; Branciforti, M.; Alves, R.; Liberman, S.; Bretas, R. Eur Polym J 2008, 44, 1346.
21. Kaito, A.; Kyotani, M.; Nakayama, K. J Macromol Sci Part B 1995, 34, 118.
22. Shah, R.; Krishnaswamy, R.; Takahashi, S.; Paul, D. Polymer 2006, 47, 6187.
23. Golebiewski, J.; Rozanski, A.; Dzwonkowski, J.; Galeski, A. Eur Polym J 2008, 44, 270.
24. Scprod.com [Internet]: Southern Clay Product Inc.; © 2006. Available at: http://www.scprod.com/product_bulletins/PB%20Cloisite%2015A.pdf.
25. Botta, L.; Scaffaro, R.; La Mantia, F. P.; Dintechva, N. J Polym Sci Part B: Polym Phys 2010, 48, 344.
26. Nazockdast, E.; Nazockdast, H. Polym Eng Sci 2008, 48, 1240.